

# Direct AC/AC Active-Clamped Converter Inductive Coupled with Half-Bridge Converter with Reduced Switches for Battery Charging Applications

Saniya Nayyar<sup>1</sup><sup>a</sup> and Manish Rathi<sup>2</sup><sup>b</sup>

<sup>1</sup>Department of Electronics and Communication Engineering, PDA College of Engineering, Kalaburagi, India

<sup>2</sup> Department of Electrical and Electronics Engineering, PDA College of Engineering, Kalaburagi, India

**Keywords:** Power Factor Correction, Cuk Converter, Fuzzy Logic Controller, Electric Vehicle Applications, Battery Charging.

**Abstract:** In this study, a novel series-series compensated inductive coupling-based battery charging system is suggested. It uses an innovative direct AC/AC active-clamped converter paired with a half-bridge converter. By removing the correction stage, the suggested converter achieves a real single stage (AC-to-AC) conversion using fewer switching devices. Additionally, it does away with the need for large, life-limited electrolytic DC-link capacitors. The suggested converter's operating modes and control structure are briefly examined. Additionally, a novel predictive dead-beat grid current control method and the linear mean current charging are created for the proposed converter, allowing for the management of charging current and a unity power factor. The simulation is to be carried out in MATLAB/Simulink software. A hardware model is designed to validate the design of the proposed system.

## 1 INTRODUCTION

Inductive power transfer (IPT) technique is becoming more widely used in a wide range of products, including electric vehicle (EV) charging, lightweight electronics, and biomedical implants. Facilitation, safety, and the potential for range enhancement are all benefits of using IPT in EV charging systems since fully automated charging gives EVs more opportunities to charge. In its most basic form, an IPT charging method consists of a pair of inductive coupling coils (Ramezani et al., 2019) compensation structures, primary converters that provide high-frequency supplies and a secondary rectification that changes the AC power into DC power for charging the battery pack (Liu et al., 2018).

In the base assembly of IPT systems, while power factor correction (PFC) is required during conversion between AC primary voltage to DC voltage in order to ensure the quality of AC input power, dual-stage conversion (AC-DC-AC) was often used until recently. After that, high-frequency inputs are

produced and sent to the primary coil by a high-frequency inverter that is coupled to the PFC rectification by a DC-link capacitor (Samanta et al., 2019).

The fundamental benefit of IPT systems employing dual-stage converter is that both the PFC rectification device and the power inverter may be independently adjusted to optimise particular performance indices since they are isolated via the DC-link capacitor. Still, the system's price, size, and weight are all increased by the existence of many converter stages and a large DC-link capacitor (Phuoc Sang Huynh et al., 2019). The usage of matrix conversions (MCs) to supply IPT systems has come under more and more scrutiny in the past few decades. MCs improve system efficiency with regard to power density, validity, and expenditure by enabling the instantaneous conversion of frequencies low AC sources (50-60 Hz) over high-frequency outcomes (up to 85 kHz) eliminating intermediary conversion phase (Moghaddami, 2018).

<sup>a</sup> <https://orcid.org/0009-0002-2453-304X>

<sup>b</sup> <https://orcid.org/0009-0005-4809-3642>

The DC-link storage modules on the main side of the single-phase matrix converter-based IPT systems are removed in order to neutralise dual frequency ripple, which causes it shown on the battery end. Batteries may be supplied by dual frequency (100 or 120 Hz) power using the sine wave ripple current (SRC) recharging approach, according to with very negligible negative impacts on performance. As a result, IPT systems based on matrix converters may benefit from the sinusoidal charging approach and do without the middle DC-link capacitor. Creating a control strategy for regulating power and correction of power factors is the main difficulty when utilising MCs for IPT charging devices (Huynh et al.,2020).

A supplementary interactive full bridge rectification is utilised in an IPT recharging device that is supplied by a buck-derived MC. The rectifier's output power can be modulated by modulating the MC using a phase-shift PWM technique. For the IPT structures, a boost-derived full-bridge MC (FBMC) that is compatible with the main parallel-series correction system is suggested (Yao et al.,2017). With dual loops of control that resemble those of a typical boost converter, the suggested converter architecture can regulate the flow of power and form main current. Additionally, a single-stage design merging a full-bridge VSI and a bridgeless boost PFC converter is suggested for IPT systems.

The main current control circuit is abolished when the converter is used in a discontinuous conduction (DCM). Nevertheless, with DCM, the converter has additional stress, losses, and EMI issues. The need for several active switches and complicated switching algorithms are the fundamental shortcomings of the previous single-stage converter architectures (Vu et al.,2019).

The IPT-based charging of batteries system is suggested to be fed by a brand-new AC/AC active-clamped converter featuring a half bridge converter on the back end. The suggested converter offers single-stage energy conversion by doing away with the front-end rectification and galvanic dc-link capacitor, which enhances the system's functionality in terms of effectiveness, dimensions, weight, and price. The main side of the converters must have a serial equalisation circuit since the converter's outcomes is high-frequency energy (Charthad et al.,2018). To improve the system effectiveness and prevent the discontinuous conductance phenomena caused by the nonlinear feature in diode-bridge rectifier devices, a dynamic rectifier is utilised in place of them on the battery side. It is created a dual regulation approach that combines regular mean current regulation with predicted deadbeat current

regulation. The use of the prediction based dead-beat (PDB) controller for line current regulation has certain advantages, including improved power factor, simple setup without taking into account load and mutual inductance fluctuations, and quick reference monitoring. In an attempt to decrease the quantity of switches as well as high frequency switching distortions, simultaneously reversible switches are substituted with a single switch connected to a rectifier bridge.

## 2 SYSTEM DESCRIPTION

The block diagram of the proposed system is shown below in Fig 1.

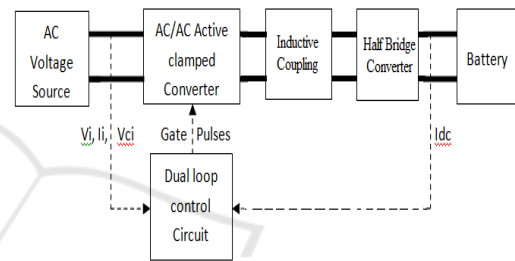


Fig 1: Proposed system Block diagram.

To power the battery in this, an ac supply is linked to the suggested converter. The battery serves as the load in this. The voltage is increased using the Ac/Ac active clamped conversion device in accordance with the load requirements, and the rate of supply is changed to a high frequency so that inductively coupled transfer of power is superior with higher frequencies. The half bridge converter receives the transmitted power and converts it from ac to dc. To ensure an effortless charging process and prevent a dual frequency fluctuation (100Hz), a dual loop regulation is offered to adjust the mean current at the pack's side. The addition of a dead-beat controller enhances the system's overall dynamic performance.

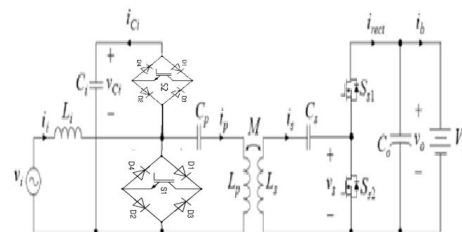


Fig 2: AC/AC Converter.

The suggested AC/AC converter combines an HB matrix converter and an AC/AC boost converter. The AC/AC converter is set up using two switches connected to diode bridges. The input current rectification and recharging regulation procedures in the suggested IPT system are accomplished by regulating the main AC/AC converter's cycle duration using dual loops of control. Both switches S1 and S2 function in positive as well as negative phases and are complimentary to one another. The proportion of the duration of the switch S1's on-time to the switching phase is known as the duty cycle, which stands for the AC/AC converter.

A high-frequency unipolar square wave voltage ( $V_p$ ), whose magnitude and direction fluctuate on the clamped voltage ( $V_{Ci}$ ), is the resultant voltage of an instantaneous AC-AC active-clamped HB converter. The SS compensating system is used because it is straightforward, affordable, highly efficient, and compensates for loads independently. The two main resonant networks are set to the identical resonant frequency, which is equivalent to the frequency of the power electronic switch, so as to maximise the electrical power deliver capabilities and reduce the VA grade of the converter. The secondary component of the network has a proactive HB rectifier, and both switches that operate Ss1 and Ss2, function at  $f_s$  with a set duty period of 0.5.

The generated duty cycle of 0.5 at the secondary voltage  $V_s$ . Remember that the higher switch Ss1's on-time to switching duration is referred to as the required period  $d_s$  of the converter. Both the resonant networks have been adjusted to the switching frequency and the phase offset across  $v_p$  and  $v_s$  is required to be held from 0 to 180 degrees in enable to transmit energy between the grid and battery pack.

$$\omega_s = 1/\sqrt{L_p C_p} = 1/\sqrt{L_s C_s}$$

Where  $L_p$  and  $L_s$  are the self-inductances of the primary and secondary coils,  $C_p$  and  $C_s$  are the primary and secondary compensation capacitors, and  $\omega_s = 2\pi f_s$  is the switching angular frequency.

The modes of operation of the proposed converter is provided below:

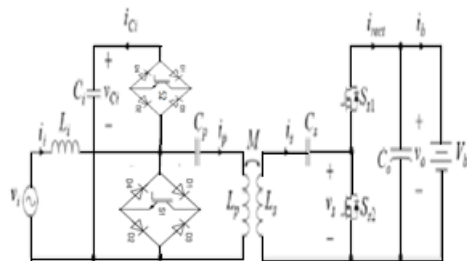


Fig 3a: Proposed Converter.

Mode 1:

The switch S1 is turned ON in this mode. The L1 gets charged by the input source. The Cp discharges and provides energy to the inductor Lp. In secondary Ss1 is ON and the inductor Ls provides energy to the load through Cs.

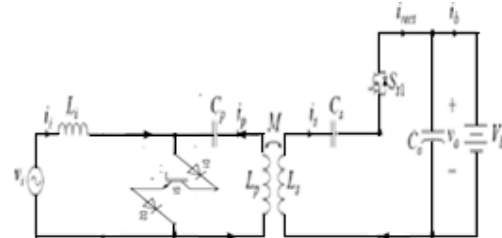


Fig 3b: Mode 1 of the Proposed Converter.

Mode 2:

The switch S1 is still turned ON in this mode and L1 gets charged by the input source along with Cp. In secondary Ss1 is ON and the inductor Ls provides energy to the load through Cs.

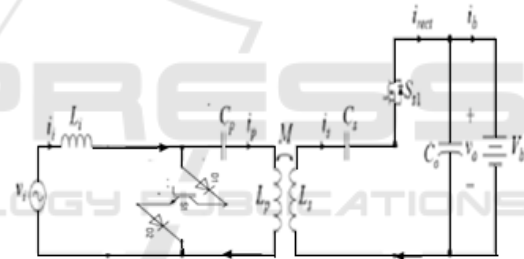


Fig 4: Mode 2 of the Proposed Converter.

Mode 3:

The switch S1 is OFF and S2 is turned ON in this mode and L1 gets discharged and charges C1 along with Cp. In secondary Ss1 is ON and the inductor Ls provides energy to the load through Cs.

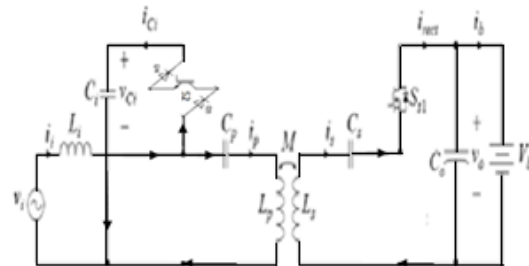


Fig 5: Mode 3 of the Proposed Converter.

**Mode 4:**

The switch S1 is OFF and S2 is turned ON in this mode and L1 gets disconnected as it completely discharged and C1 starts discharging and charges the Cp. In secondary Ss1 is ON and the inductor Ls provides energy to the load through Cs.

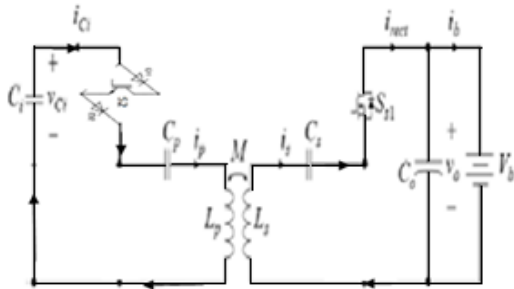


Fig 6: Mode 4 of the Proposed Converter.

**Mode 5:**

The switch S1 is OFF and S2 is turned ON in this mode and L1 gets disconnected as it completely discharged and C1 starts discharging and charges the Cp. In secondary Ss2 is ON and the inductor Ls is getting charged from Cs.



Fig 7: Mode 5 of the Proposed Converter.

**Mode 6:**

The switch S1 is OFF and S2 is turned ON in this mode and L1 gets disconnected as it completely discharged and C1 gets charged by the Cp. In secondary Ss1 is ON and the inductor Ls is getting discharged through Cs.

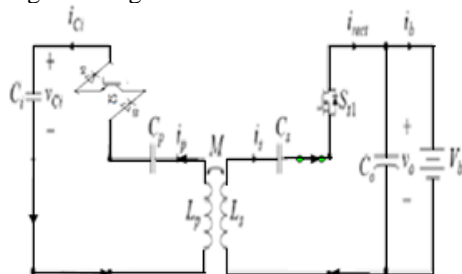


Fig 8: Mode 6 of the Proposed Converter.

For negative half cycle, the same process is repeated.

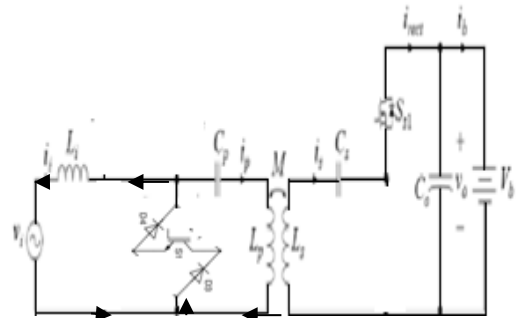


Fig 9: Mode 7 of the Proposed Converter.

**Mode 7:**

The switch S1 is turned ON in this mode. The L1 gets charged by the input source in reverse direction. The Cp discharges and provides energy to the inductor Lp. In secondary Ss1 is ON and the inductor Ls provides energy to the load through Cs.

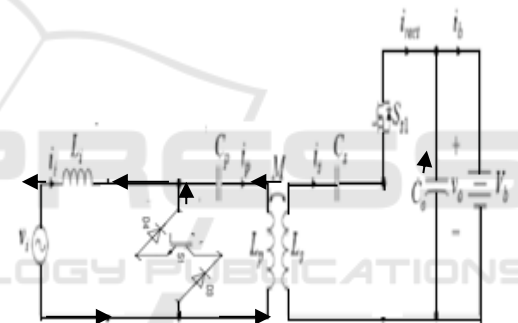


Fig 10: Mode 8 of the Proposed Converter.

**Mode 8:**

The switch S1 is still turned ON in this mode and L1 gets charged by the input source along with Cp in reverse direction. In secondary Ss1 is ON and the inductor Ls provides energy to the load through Cs.

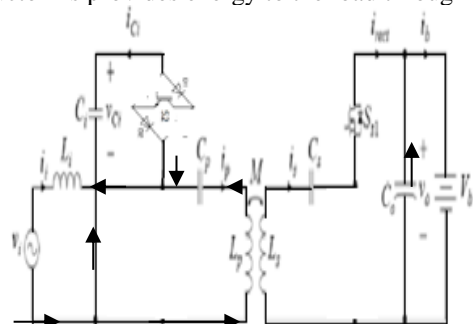


Fig 11: Mode 9 of the Proposed Converter.

Mode 9:

The switch S1 is OFF and S2 is turned ON in this mode and L1 gets discharged along with C1 and charges Cp. In secondary Ss1 is ON and the inductor Ls provides energy to the load through Cs.

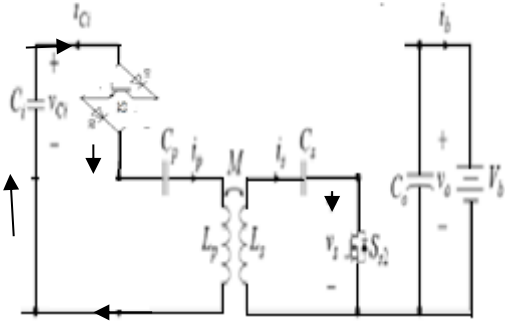


Fig 12: Mode 10of the Proposed Converter.

Mode 10:

The switch S1 is OFF and S2 is turned ON in this mode and L1 gets disconnected as it completely discharged and C1 starts discharging along with Lp and charges the Cp. In secondary Ss2 is ON and the inductor Ls getting charged from Cs.



Fig 13: Mode 11 of the Proposed Converter.

Mode 11:

The switch S1 is OFF and S2 is turned ON in this mode and L1 gets disconnected as it completely discharged and C1 starts discharging along with Lp and charges the Cp. In secondary Ss1 is ON and the energy in inductor Ls is discharged to load through Cs.

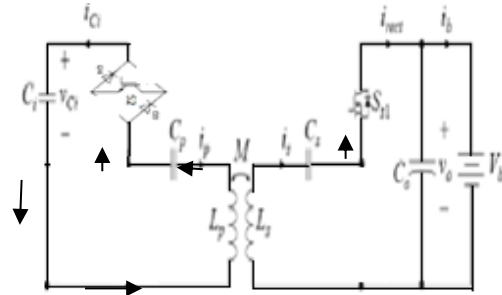


Fig 14: Mode 12 of the Proposed Converter.

Mode 12:

The switch S1 is OFF and S2 is turned ON in this mode and L1 gets disconnected as it completely discharged and C1 starts charging along with Lp from Cp. In secondary Ss1 is ON and the energy in inductor Ls is discharged to load through Cs.

A duty ratio is calculated to reduce the peak value of the capacitor clamping voltage for the peak source voltage is provided below

$$D_{pm} = V_m / V_{cm}$$

The source ripple current,  $\Delta I_m$ , for peak source voltage is provided below

$$L_i \geq \frac{(1 - D_{pm}) V_m}{\Delta I_m f_s}$$

The M is derived for peak value of source current in which  $dp = D_{pm}$ ,  $ii = I_m$ , and  $ds = 0.5$ .

$$M = \frac{2V_b \sin \theta \sin \pi D_{pm}}{\pi \omega_s I_m \pi D_{pm}}$$

The supply side and load side compensation capacitors are calculated as shown below:

$$C_p = 1/\omega_s^2 L_p, C_s = 1/\omega_s^2 L_s$$

The clamping capacitor at the supply side, Ci, is determined according to the permissible ripple voltage  $\Delta V_c$  is as shown below.

$$C_i = \frac{\Delta Q}{\Delta V_c} = \frac{1}{\omega_s} \frac{\int_{\pi/2-\theta}^{3\pi/2-\theta} i_p d\omega_s t}{\Delta V_c} = \frac{2I_{pp}}{\omega_s \Delta V_c}$$

#### DUAL CONTROL MODULATION SCHEME.

The suggested linear AC/AC converter operates by two control loops in order to attain unity source power factor and modulate power output within the single conversion phase.

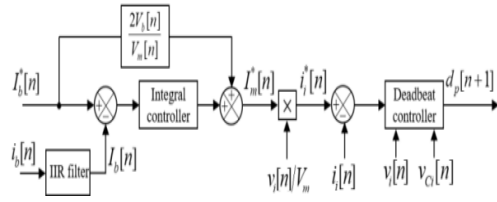


Fig 15: Dual Control Modulation Scheme.

To control the mean battery current across a line cycle, an external loop is set up. An IIR filter may be used to determine the mean current from the battery. The maximum current source reference  $I_m^*$  from the external control circuit is increased by  $v_i/V_m$  to provide the sine wave standard current  $i_i^*$  used in the internal current circuit.

The external current regulation loop, which regulates the mean current through the battery during a line cycle, generates the highest possible current source reference  $I_m^*$ . Considering the average power equilibrium at both ends of the circuit and the presumption that energy losses were ignorable, the maximum current supply reference  $I_m^*$  may be roughly calculated.

$$I_m^* = 2V_b I_b^* / V_m$$

where  $I_b^*$  is the mean value of reference battery current.

In order to achieve a unity power factor for the instantaneous AC/AC converter input, the internal control circuit is used to adjust the current source after the grid voltage. The PDB controller is used in this loop to regulate the mean switched source current. The PWM signals powering the instantaneous AC/AC converter are produced using the dual-edge/triangle regulation. By synchronising the sample at the maximum or trough for the carrier signal that is used with a particular PWM generating approach, the mean of the current source may be determined. The deadbeat regulator produces the following duty cycle:

$$d_p[n+1] = \frac{\alpha L_i}{T_s \beta v_{C_i}[n]} (i_i[n] - i_i^*[n]) + 2 \frac{v_i[n]}{v_{C_i}[n]} - d_p[n]$$

### 3 SIMULATION RESULTS

The simulation parameters of the proposed system are provided in the table given below:

Table 1.

|                      |         |
|----------------------|---------|
| Input Voltage        | 120 V   |
| Input power          | 1 KW    |
| Switching Frequency  | 85 KHZ  |
| Inductor             | 1mH     |
| Resonant Capacitor   | 11.86nF |
| Decoupling Capacitor | 3.3mH   |
| Output Capacitor     | 0.7mF   |
| Load Resistance      | 62.5Ω   |

The simulation circuit for the proposed converter is provided below:

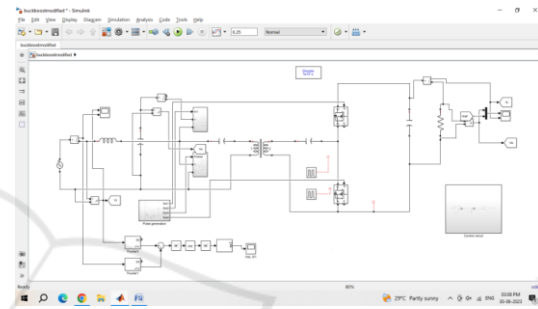


Fig 16: Simulation circuit for the proposed converter.

In this, the supply voltage of 120V is applied to the proposed converter and the load voltage reference is varied from 100V to 250 V at  $t=0.1s$ . The simulation circuit of the controller is provided below:

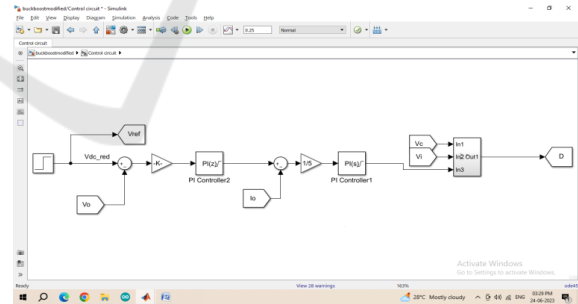


Fig 17: Simulation circuit for the proposed controller.

In this the load voltage and current is provided to the voltage control loop and current control loop respectively. The input voltage and decoupling capacitor voltage is provided to the dead beat control along with the reference current and from that duty ratio is calculated. The obtained duty ratio is provided to the pwm pulse generation and the generated pulses are provided to the controller.

The load voltage and current is provided is provided below:

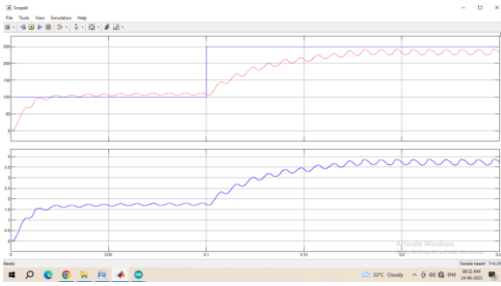


Fig 18: Load voltage and current.

In this, the reference voltage is varied from 100V to 220V at  $t=0.1s$  and the measured voltage follows the reference voltage along with the current. The power factor measured is provided below:

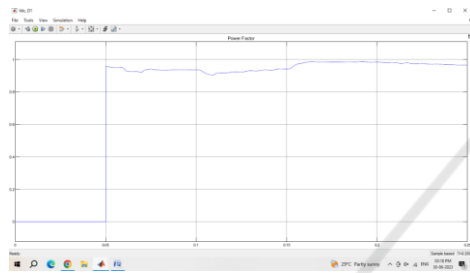


Fig 19: Power factor of the converter.

The power factor of the proposed converter is around 0.94. The %THD of the supply current is provided below:



Fig 20: THD for the proposed converter.

The %THD of the supply current is around 7.23%.

A hardware prototype model of proposed converter with input voltage of 12V, 50 Hz is developed with 48V as output voltage with load resistance of 100 ohm. The hardware parameters is provided below in the following Table II.

Table 2: Hardware Parameters.

|                        |   |
|------------------------|---|
| IRF 250N - MOSFET      | 200v, 30A                               |
| U1560-DIODE            | 200-400-600v, 15a                       |
| Capacitor              | 1000 $\mu$ F, 25V<br>1000 $\mu$ F, 100V |
| TRANSFORMER            | 12V, 1A                                 |
| TLP 250 - DRIVER IC    | 12V, 1.5A                               |
| CD 4050 BUFFER IC      | 3-18V, 0.32mA                           |
| 12V REGULATOR 7812     | 12V, 1A                                 |
| IN 4007 DIODE          | 700V, 1A                                |
| ARDUINO UNO CONTROLLER | 7-12V, 20mA                             |

Arduino uno control is used for generating the pulses for the proposed inverter and it is provided to driver circuit (TLP 250) in order to drive the mosfets IRF 250. The input voltage waveform is provided below:



Fig 21: Input voltage for the proposed converter.

The input voltage is around 14V. The load voltage waveform is provided below:

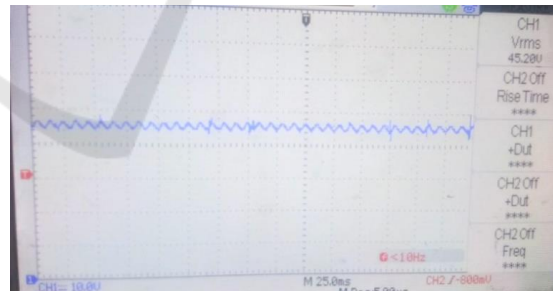


Fig 23: Load voltage proposed converter.

The load voltage is around 45.2V with voltage division as 10V/div.

## 4 CONCLUSION

In this paper, a AC/AC active clamped converter based battery charging system is presented along with operational analysis design and control structure. Additionally, a novel predictive dead-beat grid

current control method and the linear mean current charging were designed for the proposed converter, improving the power factor. The power factor is measured as 0.94 and %thd of the supply current is around 7.23%. A hardware prototype model is developed to verify the operation of the proposed converter.

Charthad, Jayant & Chang, Ting & Liu, Zhaokai & Sawaby, Ahmed & Weber, Marcus & Baker, Sam & Gore, Felicity & Felt, Steve & Arbabian, Amin. (2018). A mm-Sized Wireless Implantable Device for Electrical Stimulation of Peripheral Nerves. *IEEE Transactions on Biomedical Circuits and Systems*. PP. 1-14. 10.1109/TBCAS.2018.2799623.

## REFERENCES

- Ramezani, A., Farhangi, S., Iman-Eini, H., Farhangi, B., Rahimi, R., & Moradi, G. R. (2019). Optimized LCC-Series Compensated Resonant Network for Stationary Wireless EV Chargers. *IEEE Transactions on Industrial Electronics*, 66(4), 2756–2765.
- Liu, J., Chan, K., Chung, C. Y., Hon, N., Liu, M., & Xu, W. (2018). Single-Stage Wireless-Power-Transfer Resonant Converter With Boost Bridgeless Power-Factor-Correction Rectifier. *IEEE Transactions on Industrial Electronics*, 65(3), 2145–2155.
- Samanta, S., & Rathore, A. K. (2019). Small-Signal Modeling and Closed-Loop Control of a Parallel-Series/Series Resonant Converter for Wireless Inductive Power Transfer. *IEEE Transactions on Industrial Electronics*, 66(1), 172–182. <https://doi.org/10.1109/tie.2018.2823682>
- Samanta, S., & Rathore, A. K. (2018). A New Inductive Power Transfer Topology Using Direct AC–AC Converter With Active Source Current Waveshaping. *IEEE Transactions on Power Electronics*, 33(7), 5565–5577.
- Phuoc Sang Huynh, & Williamson, S. S. (2019). Analysis and Design of Soft-Switching Active-Clamping Half-Bridge Boost Inverter for Inductive Wireless Charging Applications. *IEEE Transactions on Transportation Electrification*, 5(4), 1027–1039. <https://doi.org/10.1109/tte.2019.2930199>
- Moghaddami, M., & Sarwat, A. I. (2018). Single-Phase Soft-Switched AC–AC Matrix Converter With Power Controller for Bidirectional Inductive Power Transfer Systems. *IEEE Transactions on Industry Applications*, 54(4), 3760–3770.
- Huynh, Phuoc Sang & Ronanki, Deepak & Vincent, Deepa & Williamson, Sheldon. (2020). Overview and Comparative Assessment of Single-Phase Power Converter Topologies of Inductive Wireless Charging Systems. *Energies*. 13. 2150. 10.3390/en13092150.
- Yao, Yousu & Wang, Yijie & Liu, Xiaosheng & Lin, Fanfan & Xu, Dian. (2017). A Novel Parameter Tuning Method for Double-sided LCL Compensated WPT System with Better Comprehensive Performance. *IEEE Transactions on Power Electronics*. PP. 1-1. 10.1109/TPEL.2017.2778255.
- Vu, V.-B., Phan, V.-T., Dahidah, M., & Pickert, V. (2019). Multiple Output Inductive Charger for Electric Vehicles. *IEEE Transactions on Power Electronics*, 34(8), 7350–7368.